letters

Structure of Arf6–GDP suggests a basis for guanine nucleotide exchange factors specificity

Julie Ménétrey[1], Eric Macia[2], Sebastiano Pasqualato[1], Michel Franco[2] and Jacqueline Cherfils[1]

[1]Laboratoire d'Enzymologie et Biochimie Structurales, CNRS, Avenue de la Terrasse, 91198 Gif-sur-Yvette, France. [2]Institut de Pharmacologie Moléculaire et Cellulaire, CNRS, 660 Route des Lucioles, 06560 Valbonne, France.

Arf6 is an isoform of Arf that localizes at the periphery of the cell where it has an essential role in endocytotic pathways. Its function does not overlap with that of Arf1, although the two proteins share ~70% sequence identity and they have switch regions, whose conformation depends on the nature of the guanine nucleotide, with almost identical sequences. The crystal structure of Arf6–GDP at 2.3 Å shows that it has a conformation similar to that of Arf1–GDP, which cannot bind membranes with high affinity. Significantly, the switch regions of Arf6 deviate by 2–5 Å from those of Arf1. These differences are a consequence of the shorter N-terminal linker of Arf6 and of discrete sequence changes between Arf6 and Arf1. Mutational analysis shows that one of the positions which differs between Arf1 and Arf6 affects the configuration of the nucleotide binding site and thus the nucleotide binding properties of the Arf variant. Altogether, our results provide a structural basis for understanding how Arf1 and Arf6 can be distinguished by their guanine nucleotide exchange factors and suggest a model for the nucleotide/membrane cycle of Arf6.

Small GTP binding proteins of the ADP ribosylation factor (Arf) family are ubiquitously involved in membrane trafficking events[1]. The most divergent members of the mammalian Arf family, Arf1 and Arf6, have distinct cellular functions despite sharing 67% sequence identity[2]. Arf1 regulates the recruitment of vesicle coat polymers, including COP1, to the Golgi apparatus. No role in recruiting a vesicle coat polymer has been identified to date for Arf6, which acts at the plasma membrane where it may couple endosomal membrane traffic to aspects of actin organization[3–8] and control regulated endocytosis and exocytosis[9–11]. Arf proteins interact with various regulatory and effector proteins[12], including a growing number of guanine nucleotide exchange factors (ArfGEFs) bearing a catalytic Sec7 domain[13]. Identifying the specificity of these ArfGEFs for a particular Arf is currently an important issue for understanding the function of Arf proteins *in vivo*.

Arf proteins undergo the GDP/GTP structural cycle that is common to small GTP binding proteins, but they also feature a unique membrane driven switch. Biochemical and crystallographic studies have provided a consistent picture of how this dual nucleotide/membrane switch functions in Arf1 (refs 14–18). Arf1–GDP partitions between the cytosol and a low affinity complex with membranes, whereas Arf1–GTP associates tightly with membranes. This stable interaction is mediated by the myristoylated N-terminal helix, which flips open upon binding GTP and inserts into the lipid bilayer. Communication between the N-terminal helix and the nucleotide binding site, which are located on opposite sides of the protein, is mediated by two β-strands and a β-hairpin loop that connect the switch I and II regions (called the interswitch region hereafter; Fig. 1b)[17]. The interswitch region is
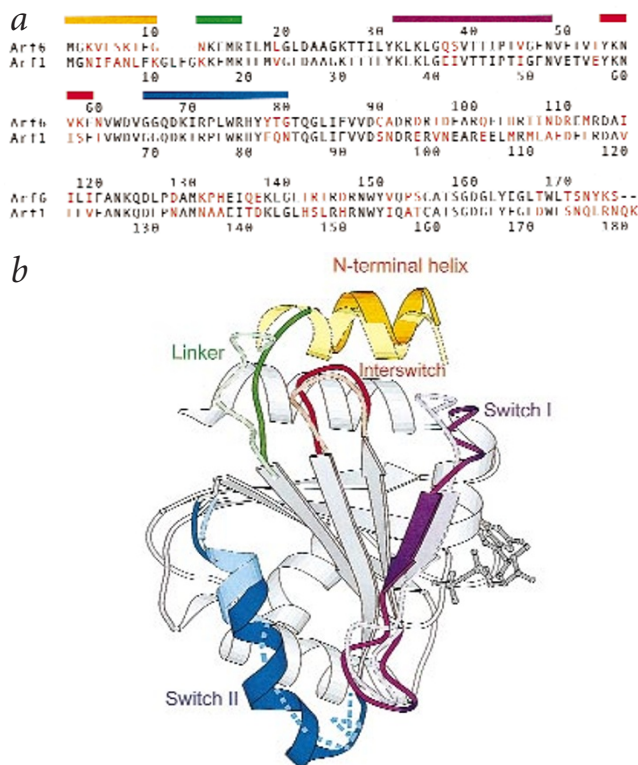

Fig. 1 Structure of Arf6–GDP. *a*, Structure-based sequence alignment. Residues that differ between Arf1 and Arf6 are in red. *b*, Superposition of Arf1–GDP[14] and Arf6–GDP. The superposition excluded the N-terminal helix and linker, the switch regions and the interswitch loop (r.m.s. deviation of Cα is 0.6 Å). Superimposable regions and the GDP nucleotide are in gray and are shown only for Arf6 for clarity. GDP is shown as a ball-and-stick model. Diverging regions are shown for both Arf1 and Arf6, with Arf6 in bright colors and a continuous outline, and Arf1 in pastel shades and a dotted outline. The N-terminal helix is yellow, the linker green, the switch I purple, the switch II blue and the interswitch loop red. The flexibility of the switch II in Arf1 is denoted by dashed lines. The figure was drawn with Molscript[36].

retracted in the protein core in Arf1–GDP and protrudes into the N-terminal helix pocket in Arf1–GTP, thus ensuring that Arf1 is activated at the surface of a membrane.

The switch I and II regions form the major sites for the interaction of Arf proteins with their cellular partners. Surprisingly, these sequences are almost identical among Arf proteins, suggesting that they may have the same three-dimensional structure. The finding that Arf6 localizes primarily to membranes, unlike Arf1 which is mostly cytosolic when bound to GDP, and that its N-terminus, which interacts with membranes in the Arf1–GTP complex, is shorter than that of Arf1, raises the possibility that its membrane/nucleotide cycle may differ from that of Arf1 (refs 19–21). Here we report the crystal structure of Arf6–GDP, which reveals that a small number of sequence differences outside the switch regions result in conformational differences between Arf1 and Arf6 in the switch regions. Mutating one of these residues, S38I (Ser 38 and Ile 42 are equivalent residues in Arf6 and Arf1, respectively), converts the GDP-binding properties of Arf6 to those of Arf1. Thus, GDP-bound Arf1 and Arf6 have different conformations. This could explain how ArfGEFs discriminate between Arf1 and Arf6 and suggests a model for the GDP/GTP cycle of Arf6.

Arf6: topology for the nucleotide/membrane switch

The crystal structure of full length, non-myristoylated Arf6–GDP
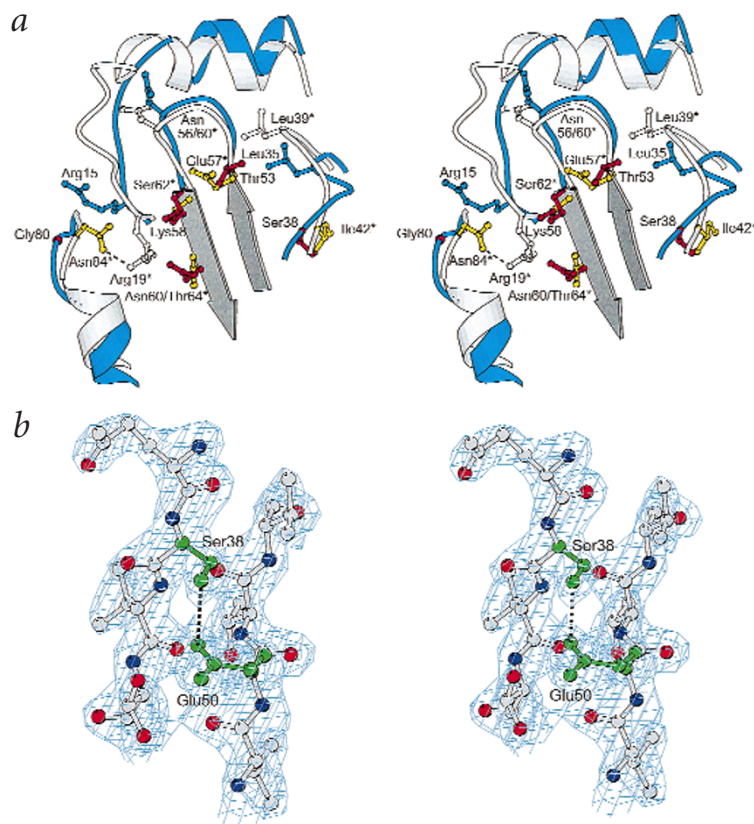
a

b

Fig. 2 Structural changes between Arf1 and Arf6. *a*, Close-up view of the most divergent regions. Arf6 is shown in blue, Arf1 in white. Differences are located at the N-terminal helix, the linker, the switch I and II regions and the interswitch loop. Sequence changes important for the distinctive conformation of Arf6 are shown in red; their counterparts in Arf1 are in yellow and are labeled with an asterisk. The β-strands in the interswitch region have similar conformations in Arf1 and Arf6 and are shown for Arf6 only (in gray). The orientation is as in Fig. 1*b*. *b*, Stereo view of the F_o - F_c electron density map near the Ser 38–Glu 50 hydrogen bond, contoured at 3σ, with shown residues omitted from the calculation.

in the switch II and interswitch regions (Fig. 2). In Arf1, Arg 19 in the linker and Asn 84 in the C-terminal region of switch II form a hydrogen bond that cannot form in Arf6 between Arg 15 and Gly 80. This leaves an empty space that is filled by the side chains of Lys 58 and Asn 60 from the interswitch region, which are bulkier than Ser 62 and Thr 64 in Arf1 and push the switch II region by its C-terminal end.

The switch I region in Arf6 is displaced essentially as a rigid body by 2 Å on average compared to Arf1–GDP (Fig. 1*b*). This displacement involves the interswitch region and an alternative interaction for Ser 38 (Ile 42 in Arf1) near the GDP binding site. The largest deviations are found upstream of switch I, up to over 5 Å near Gly 36 (Gly 40 in Arf1). Two residues, Leu 35 (Leu 39 in Arf1) and Asn 56 (Asn 60 in Arf1), which are buried in Arf1–GDP, are exposed in Arf6–GDP. This allows the interswitch region in Arf6 to pivot relative to two hinge residues, Thr53 and Lys58 (Glu57 and Ser62 in Arf1), thereby pushing the switch I by its N-terminal end. The shift of the switch I region is strengthened by a hydrogen bond between Ser 38 and Glu 50 in the interswitch region that cannot be made by Ile 42 in Arf1 (Figs 2*b*, 3*a*, see below).

In contrast, the structure of Arf6–GDP shows that regions where the sequences are different, such as the binding site for Arf GTPase activating protein (ArfGAP) in the C-terminal half of the protein[22], have the same backbone conformation in Arf1 and Arf6. Thus, regions where the sequences are divergent but the conformation is the same combine with regions of similar sequence but different conformations to build Arf proteins with unique structures.

Role of the sequence difference at Ser 38/Ile 42
The replacement of Ile 42 (Arf1) by Ser 38 (Arf6) is the only one that affects the configuration of the nucleotide binding site, driving Glu 50 (Glu 54 in Arf1) to form alternative interactions (Fig. 3*a*). The Glu 50–Ser 38 hydrogen bond in Arf6 is replaced in Arf1 by a hydrogen bond between Glu 54 and Thr 31 (refs 14,16,22), the invariant threonine that binds Mg^{2+} and the β-phosphate of GDP. Glu 54 is therefore in the coordination sphere of Mg^{2+} in Arf1 whereas Glu 50 in Arf6 is not.

To assess the role of Ser 38/Ile 42 in the affinity of Arf isoforms for GDP, we compared the kinetics of GDP dissociation from Δ17Arf1 and Δ13Arf6, with or without mutations at this position (Fig. 3*b*). At physiological Mg^{2+} concentration (1mM), Δ13Arf6 exchanged GDP about four times faster than did Δ17Arf1. Replacement of Ser 38 by Ile in Arf6 reduced the rate of GDP dissociation to its level in Arf1. Conversely, replacement of Ile 42 by Ser in Arf1 increased its GDP dissociation rate to that of Arf6.

Since Ser 38 withdraws Glu 50 from the coordination sphere of Mg^{2+} in Arf6–GDP, we studied the dissociation of GDP as a func-

was solved at 2.28 Å resolution (Fig. 1). The N-terminus, which is shorter than that of Arf1 by four residues, is folded into an α-helix that is positioned in the hydrophobic pocket opposite the nucleotide binding site, similar to that of Arf1–GDP. The missing residues do not shorten the helix as expected from sequence alignments, but instead shorten the linker that connects the helix to the protein core. As observed in Arf1–GDP, the interswitch region is buried in the protein core and interacts with the switch I region, which forms an ordered β-strand. Thus, it is likely that the structural principles for the activation of Arf6 closely mimic those for the activation of Arf1, including rearrangements of the N-terminus and the interswitch region (S.P, J.M & J.C. unpublished observations from the low resolution structure of Arf6–GTPγS). As a consequence, the localization of Arf6–GDP to membranes in cells does not arise from the inability of its N-terminal helix to bind in a pocket in the protein core (see below).

Conformation of the switch regions
The switch machinery in Arf1 comprises the N-terminal helix and its linker to the protein core, the interswitch and the switch I and II regions[14–18]. The structure of Arf6–GDP reveals that the switch components are also the regions where Arf1 and Arf6 diverge most, while other regions have essentially the same main chain conformation (Fig. 1*b*).

The switch II region of Arf6–GDP has an ordered conformation, in contrast to Arf1–GDP, which is highly flexible. Because there are only weak crystal contacts near the switch II region, it is unlikely that the conformation observed here is due to crystal packing. It forms a 3_{10}-helix as the switch II in Arf1–GTP (ref. 17; Fig. 1*b*) except that it is rotated by 25° so that the DVGGQ motif at its N-terminal end cannot bind the γ-phospate of GTP. The difference in the degree of order between Arf1 and Arf6 can be accounted for by the length of the linker, and by sequence changes
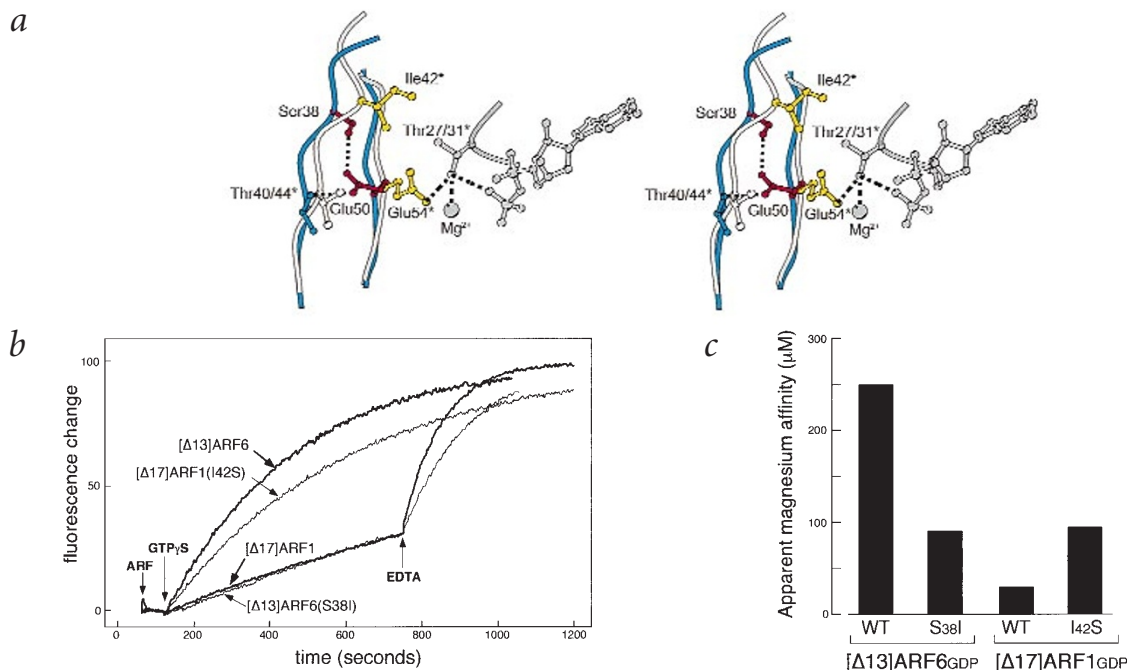
letters

a

b

c

Fig. 3 Role of the Ser 38–Glu 50 hydrogen bond. *a*, Stereo view of the interactions of Ser 38 in Arf6 and Ile 42 in Arf1. Hydrogen bonds and the interaction of Mg^{2+} with Thr31 in Arf1–GDP are indicated by dashed lines. Ser 38 forms a hydrogen bond with Glu 50, which replaces a hydrogen bond in Arf1 between Glu 54 and Thr 31. Thr 27 and GDP in Arf6 have the same conformation as Thr 31 and GDP in Arf1 and are not shown for clarity. The Mg^{2+} ion is not present in all Arf1–GDP structures, and may be replaced by an ammonium ion in Arf6–GDP. *b*, Kinetics of spontaneous GDP/GTP exchange from Δ13Arf6 and Δ17Arf1 carrying either a Ser or an Ile at position 38 (Arf6) or 42 (Arf1). Fluorescence changes are expressed as the percentage of maximal fluorescence. Measurements were performed at physiological free Mg^{2+} concentration (1 mM). GDP dissociation rates are higher for both Arf1 and Arf6 when the residue is a Ser (3×10^{-3} s^{-1} for Δ13Arf6, 6×10^{-4} s^{-1} for Δ13Arf6(S38I), 7×10^{-4} s^{-1} for Δ17Arf1 and 2×10^{-3} s^{-1} for Δ17Arf1(I42S)). *c*, Apparent affinity for Mg^{2+} of Δ13Arf6 (wild type or S38I) and Δ17Arf1 (wild type or I42S) estimated from the [³H]GDP dissociation rate as a function of Mg^{2+} concentration. A Ser residue lowers the affinity for Mg^{2+} compared to Ile for both Arf isoforms.

tion of Mg^{2+} concentration (Fig. 3*c*). The apparent affinity for Mg^{2+} was higher for Arf1 and Arf6 carrying an isoleucine than for their counterparts with a serine. Thus, the nature of the residue at position 38 (or 42 in Arf1) modulates the kinetics of GDP dissociation by allowing or preventing Glu 50 to stabilize Mg^{2+} in the nucleotide binding site; this also confirms that the structure of Arf6–GDP in the crystal is relevant to its conformation in solution. This endows the Thr 31/Glu 54 tandem in Arf1–GDP, but not Thr 27/Glu 50 in Arf6–GDP, with a role similar to that of the Ser 17/Asp 57 pair in Ras[23]. Since Glu 54 interacts with the exchange factor in the nucleotide-free complex of Arf1 with the yeast ArfGEF Gea2 (ref. 17), its alternative conformation in Arf6 may also contribute to the recognition of Arf6 by specific exchange factors.

Structural basis for the specificity of ArfGEFs

Switch regions are pivotal for the communication of small G proteins with regulatory and effector proteins. As the sequences in these regions are almost identical in Arf1 and Arf6, one would predict that they would have the same conformation and that they would not be readily distinguishable by the different proteins that interact with them. The major finding of our structural and biochemical study of Arf6–GDP is that sequence differences between Arf6 and Arf1 outside the switch regions result in structural differences in the switch regions. These differences result in distinctive nucleotide binding properties and are large enough to affect protein–protein interactions. Thus, Arf6–GDP displays structural features that allow it to be distinguished from Arf1–GDP. Major partners of GDP-bound G proteins are their GEFs. GEFs form an initial, low affinity complex with GDP-bound G proteins that isomerize to form the high affinity, nucleotide-free complex[24].

Kinetics experiments have shown that several ArfGEFs have a marked preference for either Arf1 or Arf6 that depends on their Sec7 domain[25–29], although the issue of specificity is unclear in the case of the ARNO family of ArfGEFs. The EFA6 ArfGEF, for instance, catalyzes GDP dissociation from Arf6 but does not act on Arf1 (ref. 28). In addition, the catalytic residues of Sec7 domains, which bind the switch regions of Arf proteins[17,30], display sequence variations that may influence their interactions with Arf. We propose that a certain Arf is recognized by a specific ArfGEF at the initial GDP-containing complex stage, rather than at the nucleotide-free stage. Moreover, we suggest that GDP-bound Arf1 and Arf6 are distinguishable by the different conformations and flexibility of their switch regions. Recognition by ArfGEFs of their cognate Arf proteins may also contribute to ensure that GTP bound Arfs are correctly localized, as the localization of ArfGEFs is likely to control that of Arf proteins. Subsequent isomerization of the switch regions may eventually yield a nucleotide-free transition complex in which the conformations of the switch regions in Arf1 and Arf6 become similar as in the Arf1–Gea2 complex[17], provided that specific interactions at the initial stage have prevented the isoforms from being mixed up. This also suggests that while specificity is required when Arf proteins are in the GDP-bound form, further discrimination is probably provided by the assembly of functional complexes, such as coatomers, into which incorporation of illegitimate effectors or regulators becomes unlikely.

The structure of Arf6–GDP and our comparative analysis of GDP dissociation rates also provide novel insights into the unconventional cellular cycle of Arf6. Our results reveal that Arf6 has the structural framework of the dual membrane/nucleotide switch that was described for Arf1. Thus, its predominant localization to mem-

letters

Table 1 Statistics for X-ray structure determination

Space group	P6$_1$22
Unit cell parameter	a = b = 55.66 Å, c = 194.95 Å,
	α = β = 90°, γ = 120°.
Measured reflections	76,362
Unique reflections	8,748
Completeness (%)	98.5
Resolution range (Å)	30–2.28
R$_{sym}$ (%)	6.4
R-factor (%)	17.2
R$_{free}$ (%)	23.4
R.m.s. deviations	
Bond lengths (Å)	0.011
Bond angles (°)	2.217
Average B-factor (Å^2)	17.9
Number of water molecules	92

branes, which is not affected in mutants locked in the GDP form[6], is not due to its inability to adopt the conformation that has low affinity for membranes. This observation suggests that Arf6–GDP may interact with a membrane bound protein, and such interaction may also inhibit GDP dissociation from Arf6 *in vivo*, thus preventing its higher spontaneous rate of GDP dissociation to yield constitutive activation. The only partners of GDP bound Arf proteins described to date are the βγ-subunits of heterotrimeric G proteins[9,31], whose role in the function of Arf6 is still unclear.

In conclusion, differences at the N-terminus linker combine with discrete sequence changes to define a conformation of the switch regions in Arf6–GDP that distinguish it from that of Arf1–GDP. These differences could explain how different GEFs discriminate between different Arfs. Because multiple regions contribute to the differences between Arf1 and Arf6 it is unlikely that Arf1 and Arf6 can be interconverted solely by switching their N-terminal helices. The structure of Arf6–GDP provides a striking illustration that proteins with sequence identity as high as 70% may turn out to have unexpectedly divergent conformations that are directly relevant to how they function in the cell.

Methods

Structure determination. Human ARF6 cDNA was subcloned into the pET3a vector, expressed in the BL21 (DE3) strain of *Escherichia coli* and purified to homogeneity. Arf6 was loaded with GDP prior to crystallization by incubation with 2 mM EDTA and 5 mM GDP, followed by addition of 5 mM MgCl$_2$. A unique crystal appeared after several months in a hanging drop containing equal volumes of Arf6–GDP at 5.8 mg ml^{-1} and 2 M ammonium sulfate in 0.1 M Tris/HCl at pH 8.5. Diffraction data were collected at 4 °C at the LURE synchrotron on beamline W32 (λ = 0.963 Å). Intensities were integrated with DENZO and scaled using SCALEPACK[32]. The crystal belonged to space group P6$_1$22, with one molecule per asymmetric unit and 35% solvent.

Statistics for the structure determination are summarized in Table 1. The structure was solved by molecular replacement with AMoRe[33] using Arf1–GDP (PDB accession code 1HUR) as a search model[14]. Refinement was carried out with the maximum likelihood method implemented in Xplor98 (MSI), in alternation with graphical building using TURBO-FRODO[34]. Electron density in the vicinity of the GDP phosphates was not compatible with interacting distances of Mg^{2+} (2.1–2.3 Å range), and was modeled as a NH$_4^+$ ion. Cys 155 displays additional electron density that was modeled as a dithiothreitol (DTT) molecule.

Mutagenesis and kinetics. Δ17Arf1, Δ13Arf6, Δ17Arf1(I42S) and Δ13Arf6(S38I) were expressed in *E. coli*, purified as described[35] and loaded with GDP by incubation for one hour at 37°C in the presence of 1μM free Mg^{2+} and 200μM GDP. Proteins were dialyzed

against 50 mM HEPES at pH 7.5, 100 mM KC1, 1 mM MgC1$_2$, 1 mM DTT and 5 μM GDP (HKM buffer).

Spontaneous nucleotide exchange from the different constructs was monitored by tryptophan fluorescence[35] at 37 °C with 1μM of Arf protein in HKM buffer (1mM free Mg^{2+}). The reaction was initiated by the addition of 50 μM GTPγS. As Δ17Arf1 and Δ13Arf6(S38I) have a slow spontaneous exchange, EDTA was injected after 12 min reaction in order to reach the plateau. The exchange activity was expressed as a percentage of the total amount of protein loaded with GTPγS represented by the plateau. Data were fitted as a single exponential where the rate constant is the off rate of GDP.

The apparent affinity of the different constructs for Mg^{2+} was assayed by measuring [^{3}H]GDP dissociation rates at variable concentrations of Mg^{2+} as described[15]. Briefly, Arf proteins were incubated in a twofold excess of [^{3}H]GDP (~1000 dpm pmol^{-1}) for 15 min at 37 °C in HKM buffer containing 2 mM EDTA (free [Mg^{2+}] ~1 μM). Proteins were then diluted to 1 μM in the same buffer containing free Mg^{2+} concentrations ranging from 1 μM to 10 mM. Nucleotide dissociation was monitored as the loss of protein bound radiolabel following addition of 0.1 mM GDP. The apparent affinity for Mg^{2+} was estimated as the magnesium concentration that causes 50% of the maximum variation of the rate of GDP dissociation (EC50).

Coordinates. Coordinates and structure factors have been deposited in the Protein Data Bank (accession code 1E0S).

1. Roth, M.G. *Cell* **97**, 149–152 (1999).
2. Chavrier, P. & Goud, B. *Curr. Opin. Cell Biol.* **11**, 466–475 (1999).
3. D'Souza-Schorey, C., Li, G., Colombo, M.I. & Stahl, P.D. *Science* **267**, 1175–1178 (1995).
4. Peters, P.J. *et al. J. Cell Biol.* **128**, 1003–1017 (1995).
5. D'Souza-Schorey, C., Boshans, R.L., McDonough, M., Stahl, P.D. & Van Aelst, L. *EMBO J.* **16**, 5445–5454 (1997).
6. D'Souza-Schorey, C. *et al. J. Cell Biol.* **140**, 603–616 (1998).
7. Honda, A. *et al. Cell* **99**, 521–532 (1999).
8. Radhakrishna, H., Al-Awar, O., Khachikian, Z. & Donaldson, J.G. *J. Cell Sci.* **112**, 855–866 (1999).
9. Galas, M.C. *et al. J. Biol. Chem.* **272**, 2788–2793 (1997).
10. Millar, C.A., Powell, K.A., Hickson, G.R., Bader, M.F. & Gould, G.W. *J. Biol. Chem.* **274**, 17619–17625 (1999).
11. Yang, C.Z. & Mueckler, M. *J. Biol. Chem.* **274**, 25297–25300 (1999).
12. Moss, J. & Vaughan, M. *J. Biol. Chem.* **273**, 21431–21434 (1998).
13. Jackson, C.L. & Casanova, J.E. *Trends Cell Biol.* **10**, 60–67 (2000).
14. Amor, J.C., Harrison, D.H., Kahn, R.A. & Ringe, D. *Nature* **372**, 704–708 (1994).
15. Franco, M., Chardin, P., Chabre, M. & Paris, S. *J. Biol. Chem.* **270**, 1337–1341 (1995).
16. Greasley, S.E. *et al. Nature Struct. Biol.* **2**, 797–806 (1995).
17. Goldberg, J. *Cell* **95**, 237–248 (1998).
18. Béraud-Dufour, S., Paris, S., Chabre, M. & Antonny, B. *J. Biol. Chem.* **274**, 37629–37636 (1999).
19. Cavenagh, M.M. *et al. J. Biol. Chem.* **271**, 21767–21774 (1996).
20. Yang, C.Z., Heimberg, H., D'Souza-Schorey, C., Mueckler, M.M. & Stahl, P.D. *J. Biol. Chem.* **273**, 4006–4011 (1998).
21. Gaschet, J. & Hsu, V.W. *J. Biol. Chem.* **274**, 20040–20045 (1999).
22. Goldberg, J. *Cell* **96**, 893–902 (1999).
23. John, J. *et al. J. Biol. Chem.* **268**, 923–929 (1993).
24. Cherfils, J. & Chardin, P. *Trends Biochem. Sci.* **24**, 306–311 (1999).
25. Franco, M. *et al. Proc. Natl. Acad. Sci. USA* **95**, 9926–9931 (1998).
26. Klarlund, J.K. *et al. J. Biol. Chem.* **273**, 1859–1862 (1998).
27. Claude, A. *et al. J. Cell Biol.* **146**, 71–84 (1999).
28. Franco, M. *et al. EMBO J.* **18**, 1480–1491 (1999).
29. Morinaga, N., Adamik, R., Moss, J. & Vaughan, M. *J. Biol. Chem.* **274**, 17417–17423 (1999).
30. Béraud-Dufour, S. *et al. EMBO J.* **17**, 3651–3659 (1998).
31. Franco, M., Paris, S. & Chabre, M. *FEBS Lett.* **362**, 286–290 (1995).
32. Otwinowski, Z. In *Data collection and processing* (eds Sawyer, N.I.L. & Bailey, S.) 56–62 (SERC Daresbury Laboratory, UK; 1993).
33. Navaza, J. *Acta Crystallogr. A* **50**, 157–163 (1994).
34. Roussel, A. & Cambillau, C. In *Silicon graphics geometry partners directory* (ed. Silicon Graphics) 81 (Silicon Graphics, Mountain View, California; 1991).
35. Antonny, B., Béraud-Dufour, S., Chardin, P. & Chabre, M. *Biochemistry* **36**, 4675–4684 (1997).
36. Esnouf, R.M. *Acta Crystallogr. D* **55**, 938–940 (1999).